Salts of Lanthanide(III) Hexafluoroacetylacetonates [Ln = Sm(III), Eu(III) and Tb(III)] with Dipyridylammonium Cations: Synthesis, Characterization, Photophysical Properties and OLED Fabrication

Rashid Ilmi,*[a] Danyang Zhang,[b] Leonardo Tensi,[c] Houda Al-Sharji,[a] Nawal K. Al Rasbi,[a] Alceo Macchioni,*[c] Liang Zhou,*[b] Wai-Yeung Wong,*[d] Paul R. Raithby,*[e] and Muhammad S. Khan[a]*

[a]Department of Chemistry, Sultan Qaboos University, P. O. Box 36, Al Khod 123, Oman

[b]State Key Laboratory of Rare Earth Resource Utilization, Changchun Institute of Applied Chemistry, Chinese Academy of Sciences, Renmin Street 5625, Changchun 130022, People's Republic of China.

[c]Department of Chemistry, Biology and Biotechnology and CIRCC, University of Perugia, Via, Elce di Sotto 8, 06123 Perugia, Italy

[d]Department of Applied Biology and Chemical Technology and Research Institute for Smart Energy, The Hong Kong Polytechnic University, Hung Hom, Kowloon, Hong Kong, People's Republic of China.

[e]Department of Chemistry, University of Bath, Claverton Down, Bath BA2 7AY, UK.

E-mail addresses and ORCID ID of corresponding authors:

Rashid Ilmi (RI)	: rashidilmi@gmail.com; 0000-0002-5165-5977
Muhammad S. Khan (MSK)	: msk@squ.edu.om; 0000-0001-5606-6832
Alceo Macchioni (AM)	: alceo.macchioni@unipg.it; (0000-0001-7866-8332)
Liang Zhou (LZ)	: zhoul@ciac.ac.cn; 0000-0002-2751-5974
Wai-Yeung Wong (WYW)	: wai-yeung.wong@polyu.edu.hk; 0000-0002-9949-7525
Paul R. Raithby (PRR)	: p.r.raithby@bath.ac.uk; 0000-0002-2944-0662

Abstract: A series of tetrakis lanthanide complexes with the general formula $[Ln(hfaa)_4]^{-}(DpaH)^{+}$ [Ln = (**Sm-1**), (**Eu-1**) and (**Tb-1**)], hfaa = hexafluroacetylacetonate and Dpa -2,2'-dipyridylamine] has been synthesized by the reaction of $LnCl_3$, hfaa and Dpa in the presence ammonia solution (25%). The complexes have been characterized by analytical and spectroscopic methods. The solution molecular structure of the complexes was elucidated by one- and two-dimensional NMR spectroscopy which shows that the $DpaH^{+}$ cation retains a close interaction with the lanthanide anion in solution. The crystal structure of **Eu-1**, determined by single crystal X-ray diffraction, confirms this intermolecular interaction in the solid-state through a N-H…O hydrogen bond of 2.187 Å. In the $[Eu(hfaa)_4]^{-}$ anion the EuO_8 coordination polyhedron has a square antiprism geometry with approximate C_2-symmetry around the metal centre. Photophysical, thermal, and electroluminescent properties of the complexes have been investigated. The **Sm-1** and **Eu-1** complexes displayed efficient typical red emission with a sizeable photoluminescence quantum yield (PLQY) while **Tb-1** displayed near-white light emission. The complexes have been used as dopants to fabricate single- and double-emitting layer (EML) OLEDs through the thermal evaporation method. At the optimum doping concentration, ~~the~~ double-EML **Eu-1** based device displayed orange electroluminescence (EL) with a brightness (B) of 417 cd/m^2 and very low $V_{turn\text{-}on}$ = 3.4 V. Interestingly, the **Sm-1** based single-EML device exhibited pure red emission with the *Commission internationale de l'éclairage* [$(CIE)_{x,y}$ = 0.613, 0.321], which is rare. The **Sm-1** based device performance [B = 145 cd/m^2, current efficiency (η_c) = 0.35 cd/A, power efficiency (η_p) = 0.15 lm/W with an external quantum efficiency (EQE) = 0.3% and $V_{turn\text{-}on}$ = 7.1 V] surpassed that of the only reported Sm-based single red-OLED (R-OLED).

Keywords: Hexafluoroacetylacetone; Lanthanide tetrakis complexes; Red emission; Red and Orange electroluminescence

1. Introduction

Efficient photoluminescent trivalent lanthanide [Ln(III)] complexes, especially Eu(III)/Tb(III)/Sm(III) complexes represent an important class of materials because of their unique inherent ability to emit ion-specific highly monochromatic visible (Vis) light [1]. However, 4f – 4f electronic transitions are forbidden according to the Laporte selection rule [2] resulting in low molar absorptivity (ε) or oscillator strength of the transitions [3]. Generally, this bottleneck can be surpassed by using appropriate organic ligand(s) ("*antenna*") with high ε value either in the ultraviolet (UV) or Vis region of the electromagnetic spectrum to transfer the absorbed energy to the emitting state of Ln(III), known as the "*antenna effect*" [4]. In this context, a large array of antenna ligands [4c, 5] have been utilized, among which complexes with β-diketones have been used in devices including OLEDs [1b, 6], luminescent thermometers [7], anti-counterfeit materials [8], mechanoluminescent sensors [9].

Three major classes of lanthanide complexes incorporating β-diketones as primary antenna ligand have been reported, which are; (i) $[Ln(\beta\text{-diketone})_3(solvent)_x]$ (tris complexes) [10], (ii) $[Ln(\beta\text{-diketone})_3(ancillary\ ligand)_x]$ (ternary complexes) [10-11] and (iii) $[Ln(\beta\text{-diketone})_4]^-(counterion)^+$ (tetrakis complexes) [10]. Apart from this, anhydrous and polymeric lanthanide β-diketone complexes also exist in the literature [12]. Class (i) complexes have solvent molecule~~s~~(s) in their coordination sphere, which have a detrimental effect on ~~the~~ photophysical properties. Class (ii) complexes are obtained by replacing the solvent molecule(s) by N^N- or O^O-donor ancillary ligands either by a two-step or one-step method [3a, 13]. The resulting ternary complexes display enhanced thermal stability, film-forming and most importantly, photophysical properties (PLQY reaching up to 80 – 90% [6b, 14]). In fact, the ternary complexes dominate the lanthanide coordination chemistry [6c, 10, 15]. It is also possible to replace the solvent molecule(s) by a fourth β-diketone ligand that results in anionic tetrakis complexes $[Ln(\beta\text{-diketone})_4]^-$ neutralized with various counter cations leading to class (iii) complexes [10, 16].

In continuation of our ongoing research effort to improve the EL performance of red-emitting ternary Eu(III) complexes, herein, we utilized a fluorinated β-diketone, hexafluoroacetylacetone (hfaa) as a primary antenna ligand and 2,2'-dipyridylamine (Dpa) as an ancillary ligand to synthesize class (iii) type complexes by a one-step method. The rationale for utilizing hfaa is the presence of a greater number of C–F bonds compared to high energy C-H bonds. This will curtail the radiationless transitions by vibrational relaxations and will subsequently boost the photoluminescence (PL) properties [1c, 1d, 17]. The stoichiometry used to synthesize the complexes was based on the expectation that we will isolate ternary europium complex [Eu(hfaa)$_3$(Dpa)] similar to our recently reported ternary complex [Eu(tta)$_3$(Dpa)] [18] (tta = 2-thenoyltrifluoroacetone). Contrary to our expectation, we isolated tetrakis [Eu(hfaa)$_4$]$^-$(DpaH)$^+$…(Dpa) [**Eu-1**] complex (**Chart 1**). The formulation of the complex was confirmed by elemental analysis, FT-IR, mass spectrometry and by one- and two-dimensional NMR spectroscopy. This was further attested by the solid-state structure determined by the single crystal X-ray diffraction (SC-XRD) method which confirms the formation of this unexpected tetrakis complex. Notably, reports on the synthesis of tetrakis complexes and their use as EML to fabricate OLEDs are scarce compared to ternary complexes [6c]. Given the potential optoelectronic applications and scarcity of the relevant physico-chemical-electrical data of these families of complexes, we extended the synthesis further to incorporate other visible light emitting Ln(III) ions [Ln = Sm and Tb] to obtain tetrakis complexes [Sm(hfaa)$_4$]$^-$(DpaH)$^+$ (**Sm-1**) and [Tb(hfaa)$_4$]$^-$(DpaH)$^+$ (**Tb-1**) (**Chart 1)**. All synthesized complexes were characterized by analytical and spectroscopic methods. The solution structure of the complexes was elucidated by one- and two-dimensional NMR spectroscopy. Photophysical properties of the complexes were investigated by optical absorption, emission, excitation and time-resolved spectroscopy. Thermogravimetric analysis (TGA) was employed to investigate thermal stability of the complexes, which is an important pre-requisite from the device perspectives. Finally, the complexes were used as an active emitting component to fabricate single- and double- EML orange and red OLEDs.

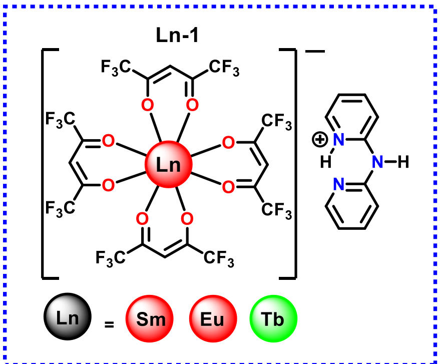

Chart 1: General chemical structures of the tetrakis complexes.

2. Experimental

2.1. Synthesis of the Complexes

Details of the chemicals, reagents and basic instrumentation are reported in the electronic supporting information (**ESI**).

2.1.1. $[Eu(hfaa)_4]^-$ $[DpaH\cdots Dpa]^+$ (Eu-1):

The tetrakis **Eu-1** complex was synthesized by the one-pot method as described below. 0.27 mL of 25% ammonia solution was diluted with 5 mL of ethanol (EtOH) and was added dropwise from a pressure-equalizing dropping funnel to an ethanolic solution (5 mL) of hfaa (0.73 g; 3.5 mmol) with constant stirring in a three-necked round bottomed flask. The reaction mixture was left to stir for thirty minutes at room temperature. After this period Dpa (0.198 g, 1.16 mmol) and $EuCl_3.6H_2O$ (0.425 g, 1.16 mmol) were separately dissolved in 5 mL of EtOH and added sequentially. The reaction mixture was left under stirring for another six hours and then left for slow solvent evaporation. After seven days a light-yellow powder precipitated out which was filtered and washed with ice-cold ethanol (3 × 5 mL) followed by hexane (2 × 5 mL) and dried in the air to obtain a yellow solid in 76% yield with respect to hfaa. It is important to emphasize that the yield of complex further improves to 81% using 1:4:1 stoichiometry. Calculated for $C_{40}H_{23}EuF_{24}N_6O_8$: C, 36.30; H, 1.75; N, 6.35; found: C, 36.25; H, 1.78; N, 6.21; FTIR (solid; cm^{-1})- ν(N-H) 3,377 cm^{-1}; $\nu(C{=}C)_{st}$ 1,646 cm^{-1}; out-of-plane asymmetric $\nu(C\text{-}F)_{st}$ 1192 cm^{-1}; in-plane $\nu(C\text{-}H)_{bend.}$ 1138 cm^{-1}; ν(C-C=C-O)+ $\nu(C\text{-}F)_{st}$ 1,097 cm^{-1} (**Fig. S1, ESI**); LC-MS: m/z = 1323.5; ^{1}H NMR (400 MHz, CD_2Cl_2, 298K, δ in ppm, J in Hz): δ = 10.63 (broad, H5), 9.35 (broad, H2), 8.74 (broad, H4), 7.91 (broad, H3), 3.41 (s, H8). ^{13}C[^{1}H] NMR (100 MHz, CD_2Cl_2, 298K, δ in ppm, J in Hz): δ = 154.6 (s, C6), 143.2 (s, C4), 140.7 (broad, C2), 119.1 (s, C3), 117.4 (s, C5), 57.5 (s, C8). ^{19}F NMR (376 MHz, CD_2Cl_2, 298K, δ in ppm, J in Hz): δ = -79.4 (s, F10).

2.1.2. $[Sm(hfaa)_4]^-[DpaH]^+$ (Sm-1):

The complex was synthesized by following the general synthetic protocol as described above for Eu-1. Yield: 70% with respect to hfaa; Calculated for $C_{30}H_{14}F_{24}N_3O_8Sm$: C, 31.31; H, 1.23; N, 3.65; found: C, 31.30; H, 1.24; N, 3.64; FTIR (solid;cm^{-1})- ν(N-H) 3,372 cm^{-1}; $\nu(C{=}C)_{st}$ 1,646 cm^{-1}; out-of-plane asymmetric $\nu(C\text{-}F)_{st}$ 1192 cm^{-1}; in plane $\nu(C\text{-}H)_{bend.}$ 1138 cm^{-1}; ν(C-C=C-O)+ $\nu(C\text{-}F)_{st}$ 1,097 cm^{-1} (**Fig. S1, ESI**); LC-MS: m/z 1230.5 for [M+ CH_3CN+ K]; ^{1}H NMR (400 MHz, CD_2Cl_2, 298K, δ in ppm, J in Hz): δ = 16.60 (broad, H1), 7.82 (d, J_{HH} = 5.2, H2), 7.59 (buried, H4), 7.58 (s, H8), 6.98 (t, J_{HH} = 6.5, H3), 6.47 (broad, H7), 5.58 (d, J_{HH} = 6.8, H5). $^{13}C[^{1}H]$ NMR (100 MHz, CD_2Cl_2, 298K, δ in ppm, J in Hz): δ = 180.5 (q, J_{CF} = 34.3, C9), 150.5 (s, C6), 141.9 (s, C4), 139.5 (s, C2), 118.2 (s, C3), 115.5 (q, J_{CF} = 287.5, C10), 113.7 (s, C5), 92.7 (s, C8). ^{19}F NMR (376 MHz, CD_2Cl_2, 298K, δ in ppm, J in Hz): δ = -76.9 (s, F10).

2.1.3. $[Tb(hfaa)_4]^-[DpaH]^+$ (Tb-1):

The titled complex was synthesized by following the general synthetic protocol as described above for Eu-1. Yield: 71% with respect to hfaa; Calculated for $C_{30}H_{14}F_{24}N_3O_8Tb$: C, 31.08; H, 1.22; N, 3.62. found: C, 31.07; H, 1.25; N, 3.64; FTIR (solid;cm^{-1})- ν(N-H) 3,337 cm^{-1}; $\nu(C{=}C)_{st}$ 1,646 cm^{-1}; out-of plane asymmetric $\nu(C\text{-}F)_{st}$ 1192 cm^{-1}; in plane $\nu(C\text{-}H)_{bend.}$ 1138 cm^{-1}; ν(C-C=C-O)+ $\nu(C\text{-}F)_{st}$ 1,097 cm^{-1} (**Fig. S1, ESI**); LC-MS: m/z 1239 for [M+ CH_3CN+ K]; ^{1}H NMR (400 MHz, CD_2Cl_2, 298K, δ in ppm, J in Hz): δ = 16.59 (broad, H1), 7.80 (d, J_{HH} = 5.1, H2), 7.57 (t, J_{HH} = 8.0, H4), 7.54 (s, H8), 6.95 (t, J_{HH} = 6.3, H3), 6.80 (broad, H7), 5.66 (d, J_{HH} = 7.6, H5). $^{13}C[^{1}H]$ NMR (100 MHz, CD_2Cl_2, 298K, δ in ppm, J in Hz): δ = 180.5 (q, J_{CF} = 34.0, C9), 150.6 (s, C6), 141.9 (s, C4), 139.5 (s, C2), 118.2 (s, C3), 115.5 (q, J_{CF} = 287.6, C10), 113.8 (s, C5), 92.7 (s, C8). ^{19}F NMR (376 MHz, CD_2Cl_2, 298K, δ in ppm, J in Hz): δ = -76.9 (s, F10).

Single crystals of **Eu-1** suitable for SC-XRD analysis were grown by the slow dichloromethane solvent evaporation method. Instrumentation and refinement details are included in the **ESI** and the data obtained are summarized in **Table S1 – S4**, ESI. CCDC contains the supplementary crystallographic data for **Eu-1**. Repeated attempts to grow single crystals of **Sm-1** and **Tb-1** for SC-XRD analysis were unsuccessful. Against this backdrop, we have elucidated the solution structure of the complexes by one- and two-dimensional NMR spectroscopy.

2.2. NMR Spectroscopy, Photophysical Parameters and OLED Fabrication:

NMR spectra of the complexes were recorded using a 400 MHz Bruker Avance III HD equipped with a smart probe. Residual solvent resonances were used for referencing and the reported chemical shifts are relative to external tetramethylsilane (TMS) (^{1}H and ^{13}C) and trichlorofluoromethane (CCl_3F) (^{19}F). Dichloromethane-d_2 (CD_2Cl_2) was used as received (EurisoTop). ^{1}H PGSE (Pulsed-Gradient Spin-Echo) NMR measurements were performed on a Bruker Avance III HD 400 spectrometer equipped with a smart probe with a *z* gradient coil, by using the standard double-stimulated echo pulse sequence without spinning [19]. The shape of the gradients was rectangular, their duration (δ) was 4 ms, and their strength (G) was varied during the experiments. All the spectra were acquired using 32k points, 16 scans and were processed with a line broadening of 1.0 Hz. The experiments were carried out with a total recycle delay of ca. 10 s. The semilogarithmic plots of $\ln\left(I/I_o\right)$ versus G^2 (a.u.) were fitted using a standard linear regression algorithm. Self-diffusion coefficients (D_t), proportional to the slope of linear fittings, were calculated using the diffusion coefficient of residual solvent resonance as an internal reference standard [20].

Important photophysical parameters for **Eu-1**: Judd-Ofelt (J-O) (Ω_2 and Ω_4) intensity parameters, radiative (A_R), non-radiative (A_{NR}) rate constants, radiative lifetime (τ_{rad}), intrinsic quantum yield (Q_{Eu}^{Eu}) and sensitization efficiency (η_{sen}) were calculated utilizing the equations (S1 – S7, ESI) and details of these calculations are discussed in our previous studies [1d]. Organic compounds utilized for the fabrication of OLEDs were procured from commercial sources and their chemical structures are shown in **Chart S1**, **ESI**. Single- and double- EML OLEDs were fabricated; details of the fabrication and instrumentation processes are included in the **ESI**.

3. Results and Discussion

3.1. Synthesis, Characterization and Crystal Structure

Generally, the stoichiometry employed for the synthesis of tetrakis lanthanide complexes is 4:4:1:1 (primary ligand:base:metal:counterion) while that for ternary lanthanide complexes is 3:3:1:1 (primary ligand:base:metal:ancillary ligand) [10]. In the present work, we intended to synthesize a new ternary Eu(III) complex incorporating hfaa as the primary ligand and Dpa as the ancillary ligand using the latter stoichiometry. The stoichiometry is based on the general assumption that the Dpa will act as a neutral bidentate ligand yielding a new ternary complex [Eu(hfaa)$_3$(Dpa)] similar to our previous report (*vide supra*) [18]. Interestingly, we isolated a tetrakis **Eu-1** (**Chart 1**) complex despite using 3:3:1:1 molar ratio of hfaa, 25% ammonia solution, Dpa and $EuCl_3.6H_2O$ in ethanol. It is well known that β-diketones exhibit keto-enol tautomerization and the extent of tautomerization depends on the polarity of the solvent and other factors [21]. Thus, a plausible explanation for the formation of this unexpected tetrakis complex could be that the β-diketone is not fully transformed into its enol form and the leftover base (ammonia solution) in the reaction mixture reacts further with the ancillary Dpa ligand transforming it into a counterion to form the tetrakis **Eu-1 complex**. Similar behaviour of the conversion of Dpa into $[DpaH]^+$ has been reported previously [16e]. Interestingly, from the analytical and NMR spectroscopic data, the Eu-1 salt was formulated as $[Eu(hfaa)_4]^-$ $[DpaH\cdots Dpa]^+$ in which the $[DpaH]^+$ cation was hydrogen bonded to an accompanying neutral Dpa molecule. To double-check that the synthesized complex is not an accidental product, we have further extended the synthesis to obtain two more new tetrakis **Sm-1** and **Tb-1** complexes using the same stoichiometry under the same experimental condition. The complexes were characterized by FT-IR, one- and two-dimensional NMR spectroscopy, mass spectrometry and elemental analyses, which explicitly confirm the tetrakis formulation of the complexes (**Chart 1**) containing $[DpaH]^+$ species as counterion, neither contained the $[DpaH\cdots Dpa]^+$ unit.

The crystal structure of **Eu-1** in **Fig. 1**, reveals a mononuclear Eu(III) centre with an 8-coordinate environment from four hfaa ligands. The $[Eu(hfaa)_4]^-$ is linked to the $[DpaH]^+$ cation by an intermolecular hydrogen bond, N-H…O 2.187 Å, N-H-O 162.77°, The crystal structure also shows the presence of a CH_2Cl_2 molecule of crystallisation in the lattice but no evidence of a neutral Dpa molecule, which is assumed to be lost in the recrystallisation process. The EuO_8 coordination polyhedron can be assigned as a distorted triangular dodecahedron, with idealised D_{2d} symmetry around the metal centre. The assignment was made using the SHAPE software package which calculates continuous shape measures (CShM's) of a set of atomic positions relative to the vertices of ideal reference polyhedral [22]. For this structure, the calculation showed a deviation of 0.46 from the idealized triangular dodecahedron and a larger deviation of 1.74 for the square antiprism. The bond distances to the Eu(III) centres are comparable to previously published ones. The Eu–O bonds are in the range 2.359(5)–2.467(5) Å (Table S3, ESI); and the *OEuO* angles are in the range of 70.4(2)– 149.5(2)º.

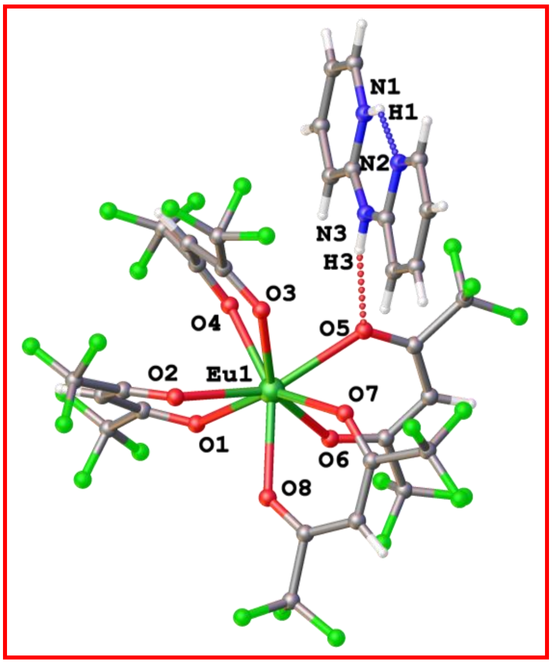

Fig. 1. The structure of **Eu-1** showing the interaction between the $[Eu(hfaa)_4]^-$ anion and the $[DpaH]^+$ cation through the intermolecular hydrogen bond between N(3)-H(3)…O(5). The solvent molecules are omitted for clarity.

3.2. Determination of Solution Structure of the Complexes

Complexes **Sm-1**, **Eu-1** and **Tb-1** were characterized in CD_2Cl_2 at 298K by a battery of mono- and bi-dimensional NMR spectroscopic techniques. The patterns of resonances of **Sm-1** and **Tb-1** are consistent with the structures shown in Chart 1. In those complexes, paramagnetism little affects the appearance of ^1H and ^{13}C spectra. As a matter of fact, all resonance are rather sharp [$\Delta\delta(^1H) \approx$ 4-6 Hz and $\Delta\delta(^{13}C) \approx$ 2 Hz] and the chemical shifts values of **Sm-1** and **Tb-1** are very similar [δ_{H8}(**Sm-1**) = 7.58 ppm and δ_{H8}(**Tb-1**) = 7.54 ppm, δ_{C8}(**Sm-1**) = 92.7 ppm and δ_{C8}(**Tb-1**) = 92.7 ppm]. A correct evaluation of the paramagnetism effect for **Eu-1** is hampered by the fact that it has a different structure. Integration of ^1H and ^{13}C resonances of **Eu-1** NMR spectra shows a 4:2 ratio between hfaa and Dpa. This leads to hypothesize the presence in solution of $[Eu(hfaa)_4]^-$ compensated by $[DpaH^{\cdots}Dpa]^+$, as discussed below.

The full NMR resonance assignment and detailed solution structural determination of **Sm-1** (Fig. 2 and Fig. S2 – S6, ESI) is discussed while NMR spectra of **Tb-1** and **Eu-1** is provided in Fig. S7 – S13 for **Tb-1** and Fig. S14 – S19 for **Eu-1**, ESI. The ^1H NMR spectrum (**Fig. S1**, ESI) shows a singlet in the aromatic region, easily identified as the CH moiety of hfaa ligand, and two doublets and two triplets due to H2/H5 and H3/H4 protons of pyridine, respectively. H4 (7.59 ppm) was identified by its long-range scalar correlation with the quaternary carbon at 150.5 ppm, reasonably assigned to carbon C6 [Fig. 2 (b)]. From the correlation pattern observable in the ^{1}H COSY NMR spectrum [Fig. 2 (a)], it was possible to assign the remaining proton resonances. Carbon resonances were assigned by means of ^{1}H, ^{13}C HSQC NMR spectrum (**Fig. S5**, **ESI**). The two NH resonances fall at very different chemical shifts (Δδ *ca*. 10 ppm). The one at high chemical shift was assigned to the protonated pyridine (H1) owing to the observation of a weak NOE with H2 (**Fig. S6**, **ESI**). Its high chemical shift value could be partially due to the establishment of a strong intramolecular hydrogen bond with the nitrogen of the other pyridine ring [23]. Interestingly, an exchange NOE is observed between the two NH protons, mediated by water, which causes the observation of NOEs for both of them and H5, in the ^{1}H NOESY spectrum (**Fig. S6**, **ESI**).

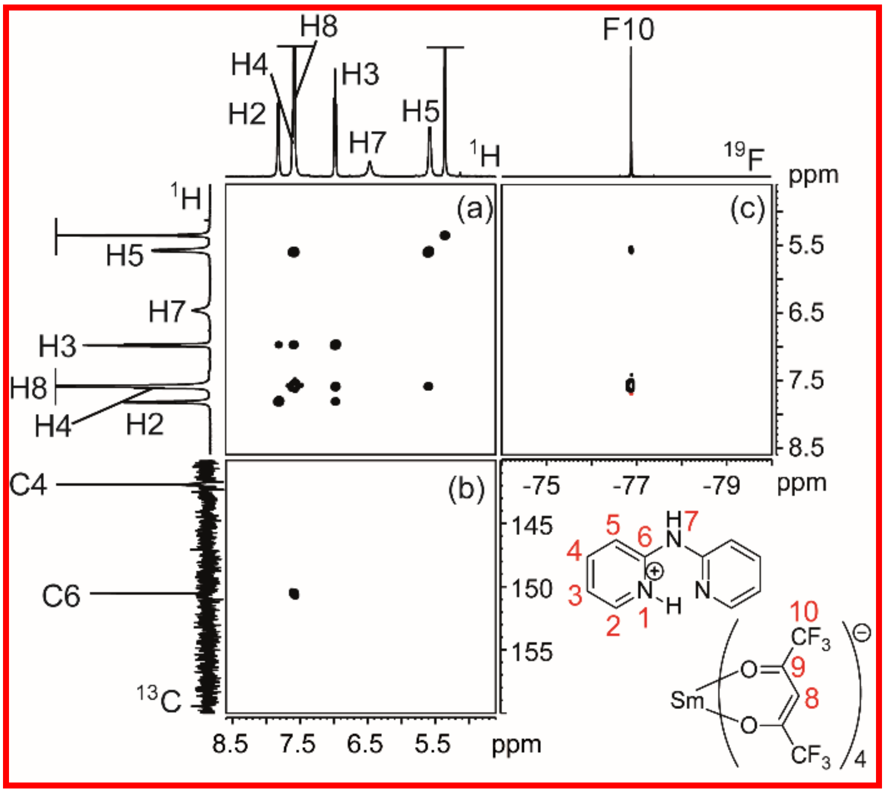

Fig. 2. Selected NMR spectra of complex **Sm-1** in CD_2Cl_2 at 298K. (a) section of ^{1}H COSY NMR spectrum, (b) section of ^{1}H, ^{13}C HMBC NMR spectrum and (c) section of ^{19}F, ^{1}H HOESY NMR spectrum.

As anticipated, the ^{1}H and ^{13}C spectra of **Eu-1** differ from those of **Sm-1** and **Tb-1**. Particularly, integration of the ^{1}H NMR resonances clearly indicates a 2:1 molar ratio between **hfaa** ligand and

Dpa. Furthermore, ^{1}H and ^{13}C resonances fall at similar chemical shift values in **Sm-1** and **Tb-1**, whereas substantial shifts are observed for **Eu-1**. Under the assumption that four **hfaa** ligands are coordinated to Eu, those observations might be explained assuming that $[Eu(hfaa)_4]^-$ is compensated by $[DpaH\cdots Dpa]^+$. The shift of the resonances on passing from **Sm-1**, **Tb-1** and **Eu-1** should be caused by pairing the $[Eu(hfaa)_4]^-$ anion with a different cation.

In order to obtain some clues on the interionic structure [24] of **Sm-1**, **Tb-1**, and **Eu-1**, ^{19}F, ^{1}H HOESY and ^{1}H PGSE NMR spectra were recorded. ^{19}F, ^{1}H HOESY NMR spectrum shows a clear interionic contact between the fluorines of $\mathbf{[Ln(hfaa)_4]^-}$ (Ln = Sm and Tb) and proton H5 of $\mathbf{DpaH^+}$ (protonated dipyridilamine), in addition to the expected intramolecular CF_3/CH contact [Fig. 2 (c)]. This suggests that the two ionic fragments are close in the space with the NH of the amine pointing toward the metal center [Fig. 3]. Interestingly, the F10/H5 contact is absent in the ^{19}F, ^{1}H HOESY NMR spectrum of **Eu-1** recorded in CD_2Cl_2, consistent with having a different compensating cation, which affects the interionic structure and, possibly, justifies the variation of the chemical shift values. The level of ionic aggregation [19-20] was evaluated by diffusion ^{1}H PGSE NMR spectroscopic experiments. The same self-diffusion translation coefficients (D_t) were determined for $\mathbf{DpaH^+}$ and $\mathbf{Ln(hfaa)^-}$, indicating that the two moieties translate together and, consequently, belong to the same even ionic aggregate [Fig. 4]. The hydrodynamic volume (V_H) derived by diffusion NMR experiments (944 Å^3 for **Sm-1**, 917 Å^3 for **Tb-1** and 1053 Å^3 for **Eu-1**), strongly suggests that ion pairs are the predominant species in CD_2Cl_2 solution. At the same time, the significantly higher V_H observed for **Eu-1** is consistent with having a larger compensating cation.

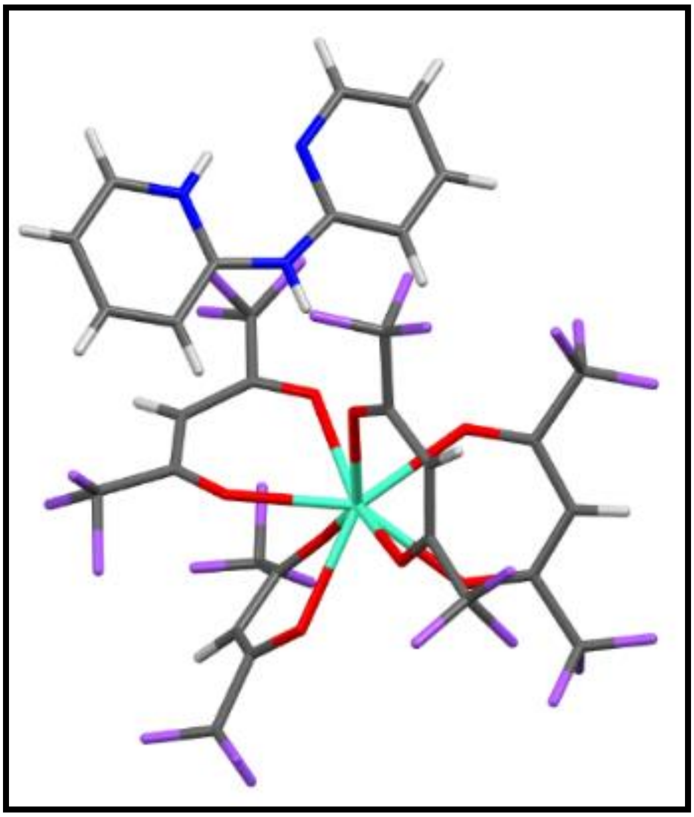

Fig. 3. The proposed general structure of **Sm-1** and **Tb-1** salts in solution (H atoms in white, C atoms in grey, N atoms in blue, O atoms in red, F atoms in purple and Sm atom in aquamarine).

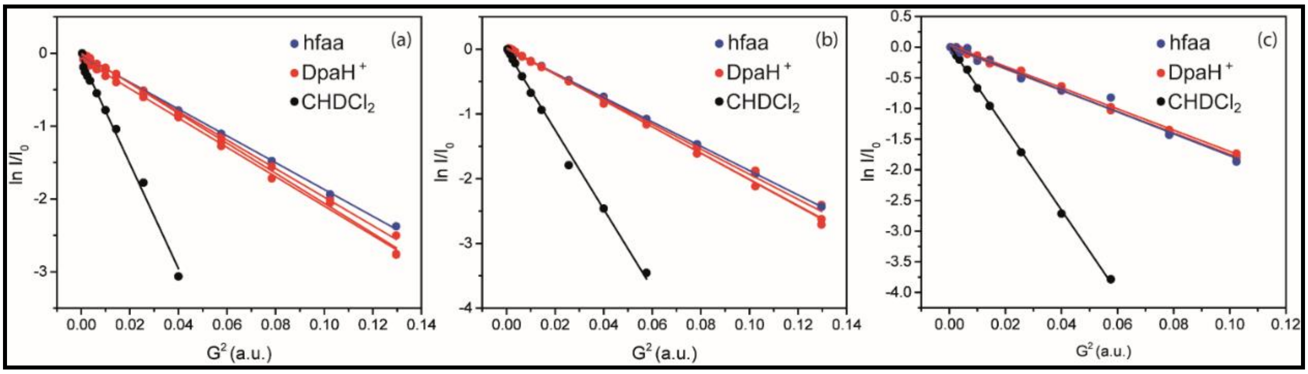

Fig. 4. Trends of ln(I/I0) vs G^2 (a.u. = arbitrary units) for the solvent (residual $CHDCl_2$, black dots), **DpaH+** (red dots) and **hfaa** (blue dots) resonances of **Sm-1** (Graph (a)), **Tb-1** (Graph (b)) and **Eu-1** (Graph (c)).

3.3. Photophysical Properties of the Complexes

For practical optoelectronic applications such as an active emitting component in OLEDs, it is necessary to know the photophysical properties of the complexes and thus we have first determined the light-absorbing capability of the complexes by optical absorption spectroscopy. The optical absorption spectra (**Fig. 5**) of the complexes were measured in dilute dichloromethane (DCM:

CH_2Cl_2). As can be seen from **Fig. 5**, the complexes displayed almost identical absorption spectra with λ_{max}^{abs} = 304 nm and is essentially an overlap of π – π* transitions of both hfaa and Dpa (310 nm) [18]. The high values of ε are 48,933, 45,844 and 43,164 $M^{-1}cm^{-1}$ for **Sm-1, Eu-1** and **Tb-1**, respectively, indicating that the synthesized complexes have a good light-absorbing capacity and we may expect to see efficient PL properties.

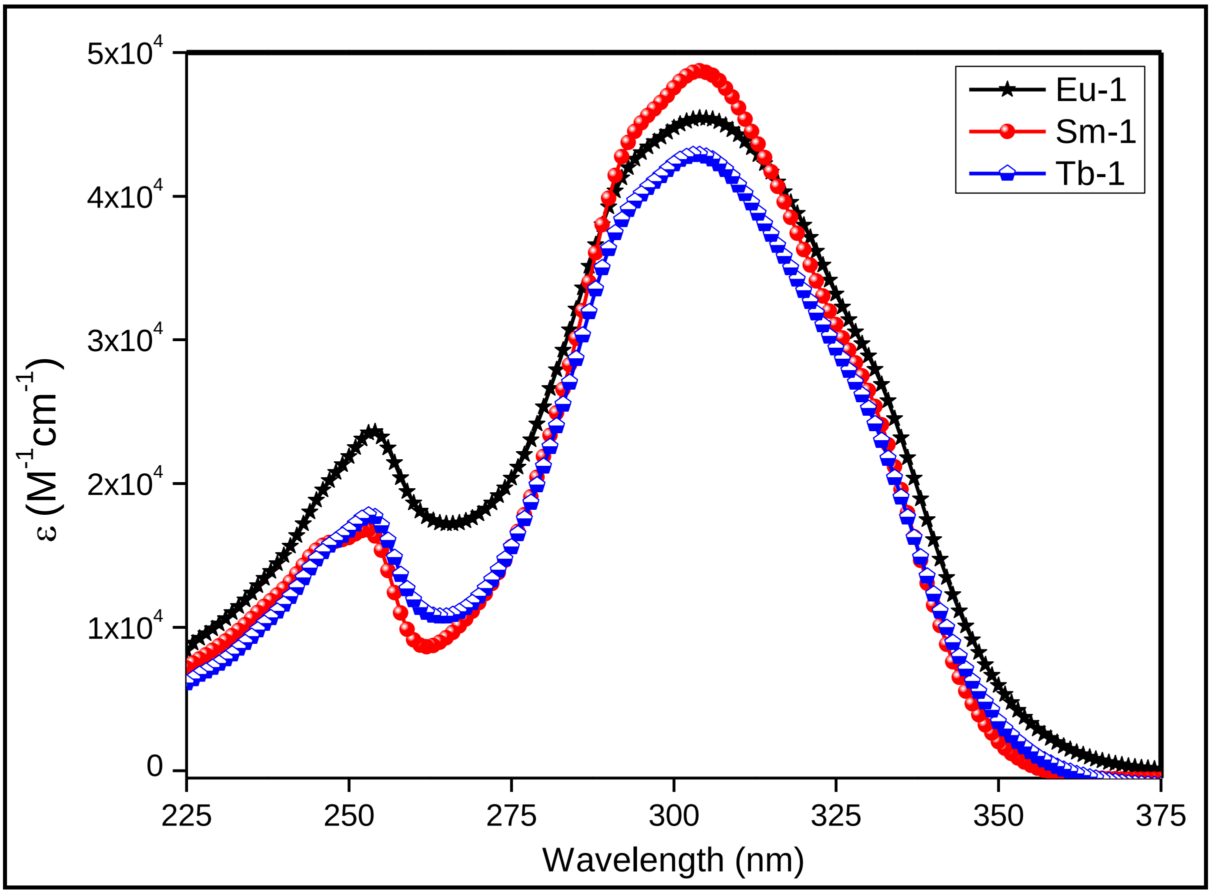

Fig. 5. Optical absorption spectra of the complexes in DCM (0.00005 M).

The excitation spectra of the complexes were determined in the solid-state by monitoring the most intense emission transitions $^4G_{5/2} \rightarrow {}^6H_{9/2}$ for Sm(III), $^5D_4 \rightarrow {}^7F_5$ for Tb(III) and $^5D_0 \rightarrow {}^7F_2$ for Eu(III), respectively (**Fig. S20, ESI**). The spectrum of **Sm-1** exhibited broad bands with some intra-configurational 4f – 4f transitions (300 – 550 nm) and was assigned [25] to $^4M_{21/2}$, $^4K_{11/2}$,$^6P_{3/2}$,$^4F_{7/2}$,$^4L_{13/2} \leftarrow {}^6H_{5/2}$ (406 nm), $(^6P,^4P)_{5/2} \leftarrow {}^6H_{5/2}$, $^4I_{11/2}$, $^4M_{19/2}$ (418 nm), $^4M_{19/2}$, $^4I_{9/2} \leftarrow {}^6H_{5/2}$ (477 m), $^4F_{3/2} \leftarrow {}^6H_{5/2}$ (527 nm), respectively (**Fig. S20, ESI**). The excitation spectra of **Tb-1** and **Eu-1** is similar to **Sm-1** except for the intra-configurational transition at 488 nm assigned to $^7F_6 \leftarrow {}^5D_4$ [1d] (**Fig. S20, ESI**) for **Tb-1** and 466 nm assigned to $^7F_0 \rightarrow {}^5D_2$ [1d] for **Eu-1,** respectively.

The emission spectrum of the **Sm-1** was obtained by choosing λ_{Ex} and exhibits typical Sm(III) emission shown in **Fig. 6** (**Please see separate Fig. S21, ESI**) in the region between 500 to 750 nm. The complex displayed four well-resolved emission transitions (**Table 1**) which are dominated by the narrow (FWHM = 9.47 nm, **Table 1**) hypersensitive electric-dipole (ED) $^4G_{5/2} \rightarrow {}^6H_{9/2}$ transition. Moreover, CIE colour coordinates calculated from the emission spectrum indicates that **Sm-1** emits vivid red emission $(CIE)_{x,y}$ = 0.613; 0.324 (**Fig. 6d**; **Table 1**) and complies well with the National Television System Committee (NTSC) ($CIE_{x,y}$ = 0.67; 0.33) suggesting its potential to be utilized as an EML to fabricate R-OLEDs. Furthermore, time-resolved PL decay of **Sm-1** exhibited monoexponential decay behaviour with a significantly longer lifetime (τ_{obs}) = 184.07 μs (**Table 1, Fig. S22, ESI**) than reported tetrakis complexes [16d, 26] and compares well with the most efficient neutral ternary complexes [1c, 27]. The solid-state absolute PLQY (Q^L_{Sm}) of Sm-1 is 4.2% which compares well to the above-mentioned highly efficient Sm(III) complexes. Moreover, from the PLQY and τ_{obs} data, we ~~have~~ further calculated the A_R and A_{NR} rate constant which are summarized in **Table 1**.

In contrast to the efficient red **Sm-1** emission, **Tb-1** displayed weak (**Fig. 6, Fig. S23, ESI**) but well-resolved emission peaks originating from the $^5D_4$ state to different ^7F_J (Please see **Table 1**). Interestingly, the complex displayed near-white light emission ($CIE_{x,y}$ = 0.245; 0.304, **Fig. 6d**) due to the presence of residual ligand fluorescence (RFL) with an excited state lifetime of 2.97ns (Fig. S24, ESI). Thus, **Tb-1** could serve as a potential candidate for the fabrication of single-component white OLEDs as noted in our recent work [28]. Moreover, it has shorter τ_{obs} = 146.46 μs (**Table 1, Fig. S25, ESI**) compared to $[Tb(hfaa)_3(H_2O)_2]$ = 530 μs [29]. This shortening could be due to the energy mismatch (ΔE = 1,500 cm^{-1}) between the triplet state of the primary hfaa antenna ligand (T_1= 21,930 cm^{-1}) [29] and $^5D_4$ (20,430 cm^{-1}) emitting state of Tb(III). This fact is further reflected in inferior ~~quantum yield~~ Q^L_{Tb} = 3.8%. This possibly could be due to the large value of A_{NR} = 6.56 × 10^3 s^{-1} (**Table 1**).

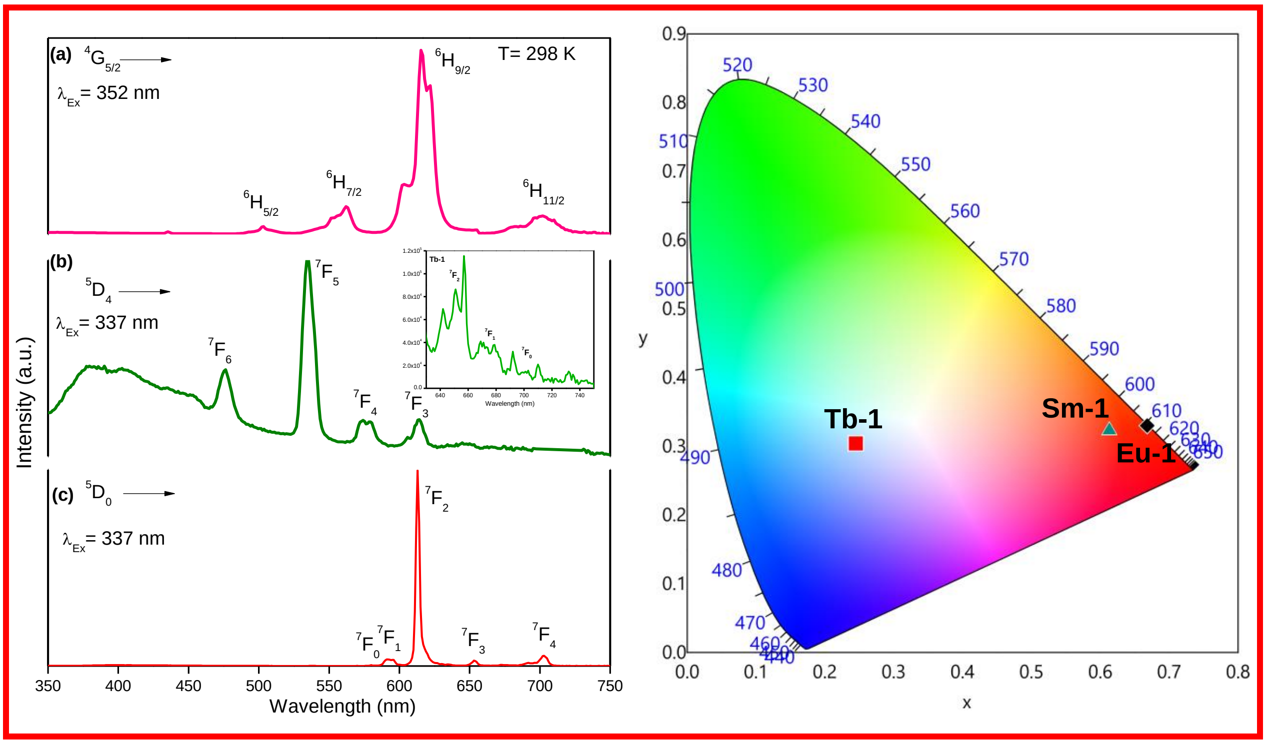

Fig. 6. Room temperature emission spectra of (a) **Sm-1** (λ_{Ex} = 352 nm), (b) **Tb-1** (λ_{Ex} .= 337 nm) with the inset showing the magnified spectrum of Tb-1 in the region between 630 – 750 nm corresponding to the $^5D_4 \rightarrow {}^7F_{2,1,0}$ transitions and (c) **Eu-1** (λ_{Ex} = 337 nm) in the solid-state. (d) CIE color diagram of the complexes.

Table 1: Room-temperature Photophysical Parameters of **Sm-1** and **Tb-1** in the solid-state.

Complex	Transition [nm;cm^{-1}]	τ_{obs} (μs)	FWHM[a] (nm)	Q^{L}_{Ln}	Q^{Ln}_{Ln}	$(A_R)^b$	$(A_{NR})^c$	$(CIE)_{x,y}$
				(%)		s^{-1}		
Sm-1	$^4G_{5/2} \rightarrow {}^6H_{5/2}$ [565; 17,699] $^4G_{5/2} \rightarrow {}^6H_{7/2}$ [609; 16,420] $^4G_{5/2} \rightarrow {}^6H_{9/2}$ [649; 15,408] $^4G_{5/2} \rightarrow {}^6H_{11/2}$ [714; 14,005]	184.07	9.47	4.2	5.9	2.28×10^2	5.52×10^3	0.613; 0.324
Tb-1	$^5D_4 \rightarrow {}^7F_6$ [490; 20,408] $^5D_4 \rightarrow {}^7F_5$ [547; 18,281] $^5D_4 \rightarrow {}^7F_4$ [587; 17,035] $^5D_4 \rightarrow {}^7F_3$ (623 ;16,051]	146.46	9.63	3.8	4.8	2.60×10^2	6.56×10^3	0.245; 0.304

[a]FWHM = Full width at half maxima of $^4G_{5/2} \rightarrow {}^6H_{9/2}$ for **Sm-1** and $^5D_4 \rightarrow {}^7F_5$ for **Tb-1**; Q^{L}_{Ln} = Absolute PLQY; Q^{Ln}_{Ln} = (Intrinsic quantum yield) = $Q^{Ln}_{Ln} = \frac{\tau_{obs}}{\tau_{rad}}$ (where τ_{rad} is the natural lifetime of lanthanide ion and is 3100 μs [30] for Sm(III) and 3000 μs [31] for Tb(III)); ^bA_R (radiative decay rate constant) $= \frac{Q^{L}_{Ln}}{\tau_{obs}}$; $^cA_{NR}$ (non-radiative decay rate constant) $= \frac{1}{\tau_{obs}} - A_R$

The PL spectrum of **Eu-1** displayed five transitions due to the deactivation of the $^5D_0 \rightarrow {}^7F_J$ presented in **Fig. 6 (Fig. S26, ESI)** and the data obtained are summarized in **Table S6, ESI**. As noted in many Eu(III) complexes, the spectrum of **Eu-1** is also dominated by the narrow (FWHM = 3.00 nm) hypersensitive ED $^5D_0 \rightarrow {}^7F_2$ (% contribution to total intensity 79.64%, **Table S6, ESI**) transition peaking at 16,281 cm^{-1} (614 nm) responsible for the brilliant red emission with the $(CIE)_{x,y}$ = 0.668, 0.330 (**Fig. 6d**, **Table 2**). Moreover, the dominance of the $^5D_0 \rightarrow {}^7F_2$ ED to a magnetic dipole (MD) $^5D_0 \rightarrow {}^7F_1$ transition implies that the dynamic coupling (DC) mechanism is the main operative mechanism in the emission process [18]. The lifetime τ_{obs} of the **Eu-1** exhibits a monoexponential decay behaviour with τ_{obs} value in millisecond (ms) regime i.e., 1.1 ms (1010 μs, **Fig. S27, ESI**). It is noteworthy that in all the complexes under study, the PL decay profile displays monoexponential behaviour and signifies the presence of single emitting species and the purity of the complexes. This is further attested by the crystal structure of **Eu-1** and NMR spectra of the complexes in solution which do not show any sign of dissociation/any other kind of complexes other than **Eu-1**. Furthermore, together with the help of the steady-state PL spectrum and τ_{obs} a range of important photophysical parameters by applying a set of equations **S1 – S7, ESI** can be calculated. The calculated photophysical parametrs are summarized in **Table 2**. From **Table 2**, it is very clear that **Eu-1** exhibits highly efficient PL with long τ_{obs}, high Q_{Eu}^{L} = 60.00 %, and Q_{Eu}^{Eu} = 92.88% which compares well with reported tetrakis complexes [16c, 26b, 32]. It is important to note the high value of the Q_{Eu}^{Eu} is due to suppression of A_{NR} = 64.74 s^{-1}. Finally, the Ω_2 and Ω_4 parameter is calculated for **Eu-1** (**Table 2**), the high values of Ω_2 = 22.02 × 10^{-20} cm^2 together with high R_{Eu} = 12.72 suggests that Eu((III) ion in **Eu-1** is surrounded by a highly polarizable environment (as in the case of β-diketone) [13a]. Parameter Ω_4 is related to the long-range effects (hydrogen bonding and π–π stacking). The substantial large value of Ω_4 ≈ 8.50 × × 10^{-20} cm^2 is indicative of these effects [6a] which is further supported by the single crystal X-ray structure that showed extensive hydrogen-bonding interactions of NH···O as well CH···F.

Table 2: Room-temperature Photophysical Parameters of **Eu-1** in the solid-state.

	Ω_2	Ω_4	FWHM[b]	τ_{obs}	τ^{c}_{rad}	A^{d}_{R}	A^{e}_{NR}	$(Q^{Eu}_{Eu})^{f}$	Q^{L}_{Eu}	η^{g}_{sen}	R^{h}_{Eu}	CIE (x,y)
Eu-1	$\times 10^{-20}$ cm^2			(μs)		(s^{-1})		(%)		(%)		
	22.02[a]	6.93[a]	3.00	1010	1184	844.35	64.74	92.88	60.00	64.60	12.72	0.668, 0.330

[a]Eq. S1; [b] FWHM (nm) = $^5D_0 \rightarrow {}^7F_2$; [c] Eq. S5; [d] Eq. S2 and S3; [e] Eq. S4; [f] Eq. S6; [g] Eq. S6; [h] ratio of $^5D_0 \rightarrow {}^7F_2/{}^5D_0 \rightarrow {}^7F_0$

3.4. EL Performance and OLEDs Chromaticity

Before OLED fabrication either by vacuum thermal evaporation or solution processing, it is necessary to know the thermal stability of the complex in question since inferior thermal stability of the complex leads to reduction of device stability especially at the peak of its use due to the Joule heating when current flows through the organic layers [33]. Against this backdrop, the thermal stability of the complexes was determined by TGA (50 – 600 °C, **Fig. 7**) under a dinitrogen (N_2) atmosphere. As can be seen from **Fig. 7**, the thermograms of the complexes do not exhibit any mass loss between 50 and 150 °C suggesting that the complexes have no lattice held or coordinated water molecules, which can be corroborated by the FT-IR, SC-XRD structure (**Eu-1**) and NMR spectroscopic studies. The decomposition temperature (T_d) with 5% weight loss of the complexes are 200 °C for **Eu-1** and 220 °C for both **Sm-1** and **Tb-1**, respectively. The relatively lower T_d of **Eu-1** perhaps could be due to the presence of the extra Dpa unit. Nevertheless, all three complexes have sufficiently high thermal stability and thus can easily be utilized to fabricate OLEDs by the vacuum thermal evaporation method.

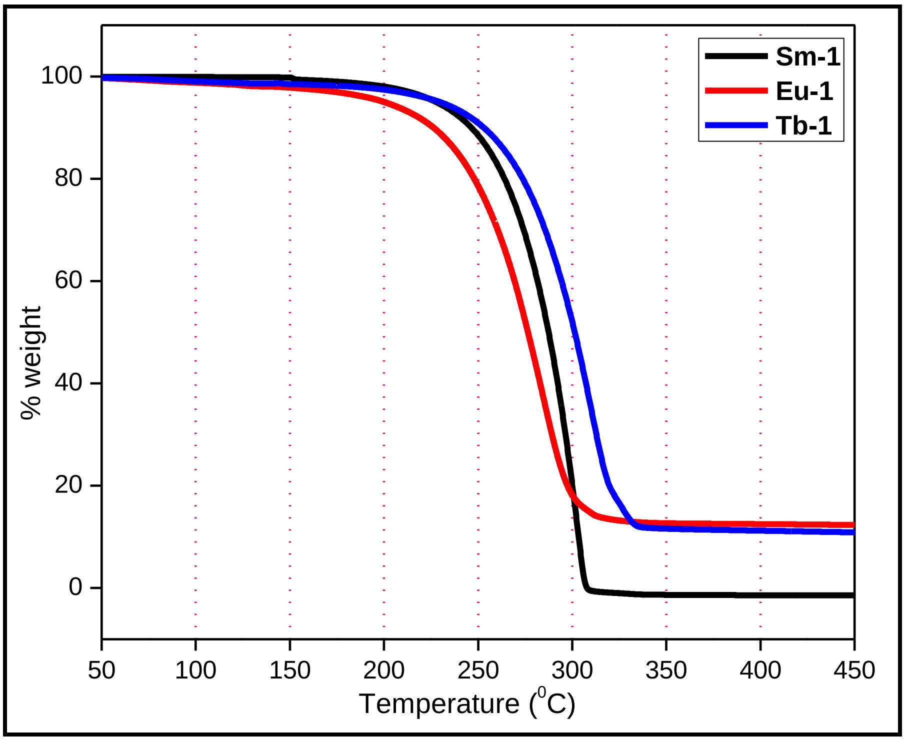

Fig. 7: TGA profiles of **Sm-1**, **Eu-1** and **Tb-1** under N_2 atmosphere.

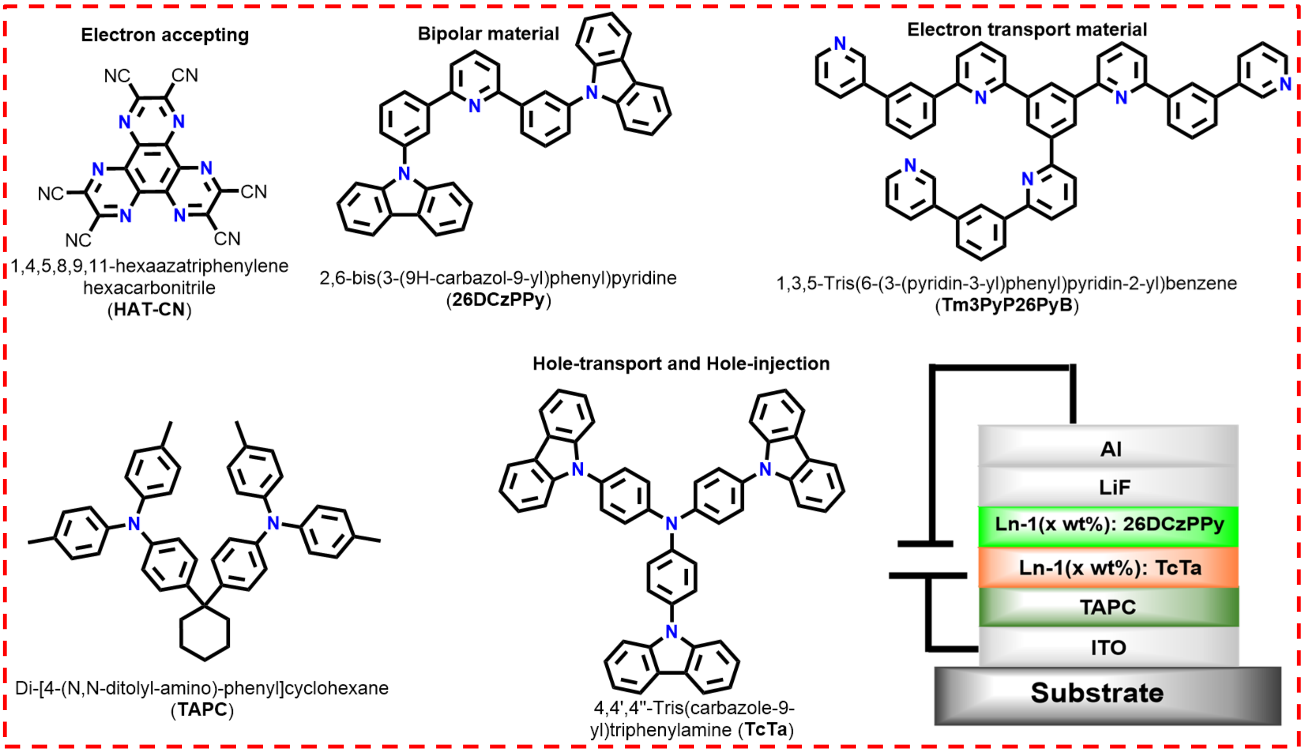

Chart 2: Chemical structures of the organic compounds utilized in the OLEDs fabrication with the general double-EML device structure.

Impressive PL efficiency (**Table 1** and **2**) and good thermal stability of the tetrakis complexes motivated us to utilize the complexes as emitters to fabricate single- and double- EML OLEDs with the general device structures for single EML OLEDs: ITO/HAT-CN (6 nm)/HAT-CN (0.2 wt%): TAPC (50 nm)/**Ln-1** (x wt%): 26DCzPPy (10 nm)/Tm3PyP26PyB (60 nm)/LiF (1 nm)/Al (100 nm) and double EML OLEDs: ITO/HAT-CN (6 nm)/HAT-CN (0.2 wt%): TAPC (50 nm)/ **Ln-1** (x wt%): TcTa (10 nm)/ **Ln-1** (x wt%): 26DCzPPy (10 nm)/Tm3PyP26PyB (60 nm)/LiF (1 nm)/Al (100 nm) *via* vacuum thermal evaporation technique (**Chart 2 and the full details of device structures in ESI in Section S3**) to investigate their EL properties. The device based on **Tb-1** displayed inferior EL performance and thus is not included in the discussion. The doping concentrations of the complexes was fine-tuned; moreover, as the doping concentration increased the temperature of evaporation also increased gradually [139 to 142 °C for **Sm-1** and 134 to 145 °C for **Eu-1**]. The low thermal evaporation temperature of the complexes thus warrants negligible decomposition during the device fabrication processes. The obtained data of B, η_c, η_p, CIE color coordinates and EQE for single-EML as well as double-EML OLEDs are summarized in **Table 3** and **Table S6, ESI** for **Sm-1** and **Eu-1**, respectively. The normalized EL spectra of the single- and double- EML devices of **Sm-1** and **Eu-1** based complexes are shown in **Fig. 8 and Fig. S28 – S30, ESI**. The EL spectra from both complexes displayed characteristic Sm/Eu(III) emissions. However, it exhibits a very minor red shift in the hypersensitive ED $^4G_{5/2} \rightarrow {}^6H_{9/2}$ and $^5D_0 \rightarrow {}^7F_2$ transitions of Sm(III) and Eu(III), respectively (**Figs. S31 & S32, ESI**). This observation could be rationalized by assuming that in the device emission process, both carrier trapping and Förster energy transfer from the host co-exist simultaneously [6b, 34]. Furthermore, EL spectra of the single- as well as double-EML devices of **Sm-1** exhibited faint ignorable emission in the UV region while for **Eu-1** the devices showed broad host emission in the region between 350 and 550 nm. Moreover, the intensity of the host emission decreases as the doping concentration increasing, implying increased carrier trapping on the Ln(III) molecules and improved ET from host to **Sm-1**/**Eu-1** molecules [1b, 6a]. At the optimum doping concentration of 4 wt%, single-EML Device **3** and double-EML Device **8** of **Sm-1** display pure red emission with $(CIE)_{x,y}$ = $(0.613, 0.321)_{\textbf{Device 3}}$ and $(0.622, 0.323)_{\textbf{Device 8}}$ color coordinates (**Fig. 9 & Fig. S33, ESI, Table 3**). However, the color emitted by the **Eu-1** based devices falls in the bright reddish-orange to orange emission (**Fig. S34 & S35** and **Table S6, ESI**) due to the presence of host emission.

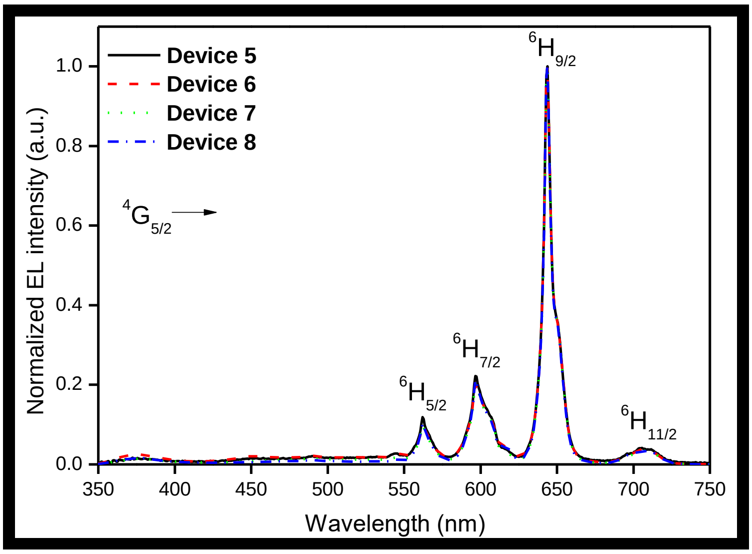

Fig. 8. Normalized EL spectra of **Sm-1** based devices **5**, **6**, **7** and **8** operating at a current density of 10 mA/cm^2.

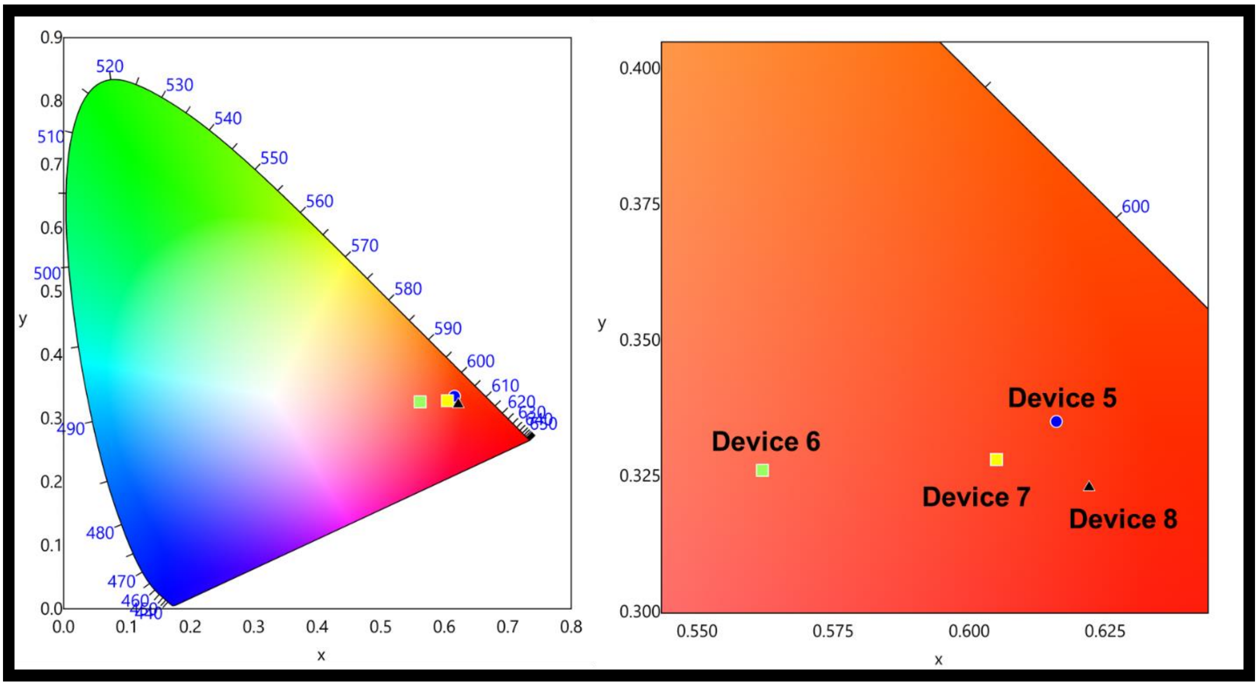

Fig. 9: CIE 1931 chromaticity diagrams of single-EML devices **5, 6**, **7** and **8** based on **Sm-1** with a magnified view at 10 mA/cm^2.

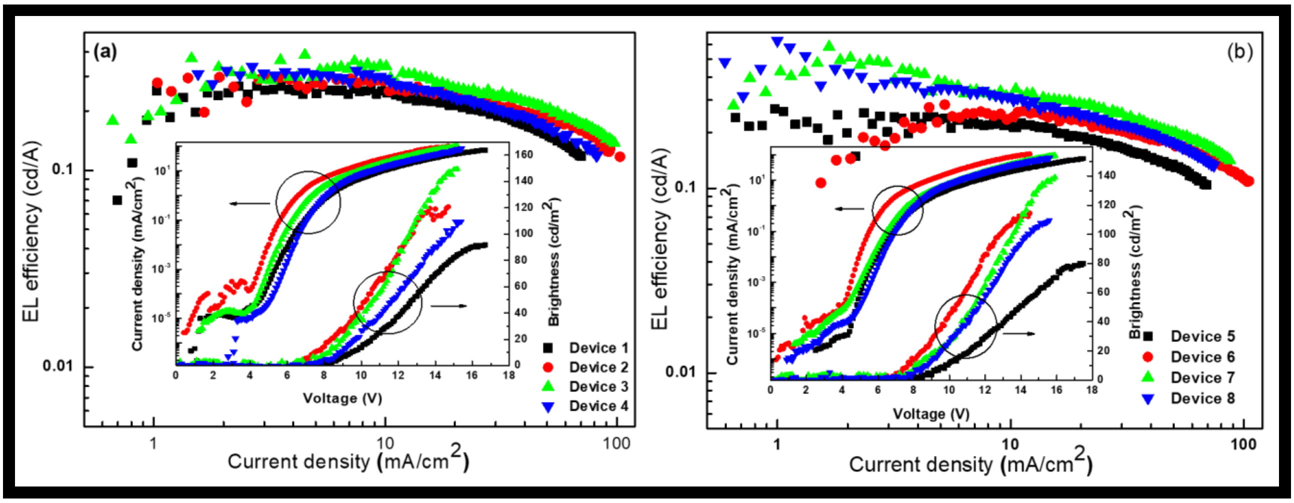

Fig. 10. EL efficiency-current density characteristics and the inset *J-B-V* characteristics of **Sm-1** based devices. (a) Devices **1**, **2**, **3** and **4** and (b) Devices **5**, **6**, **7** and **8**.

The EL efficiency and current density curves, together with the voltage (V)-brightness (B) and current density curves as an inset are shown in **Fig. 10**, and **Figs. S36 & S37**, **ESI** for **Sm-1** and **Eu-1**, respectively. The detailed EL performances such as B, η_c, η_p and EQE of single- as well as double-EML devices of **Sm-1** and **Eu-1** are summarized in **Table 3** and **Table S6, ESI**. At the optimum doping concentration of 4.0 wt%, **Sm-1** based single-EML device (Device 3) exhibited B = 145 cd/m^2, η_c = 0.35 cd/A, η_p = 0.15 lm/W with an EQE = 0.3%, $V_{turn-on}$ = 7.1 V and (CIE)x,y = (0.613, 0.321) at 10 mA/cm^2. Moreover, the inclusion of an exciton/electron blocking layer materials tris(4-carbazoyl-9-ylphenyl)amine (TcTa) in the device structure results in a minor improvement in the EL performance of the device (**Table 3**) at the optimum doping concentration 4.0 wt% (**Device 7**) of **Sm-1**. On the other hand, at the optimum doping concentration, double-EML **Eu-1** device (Device 5) displayed orange emission with EL performance B = 329 cd/m^2, η_c = 0.46 cd/A, η_p = 0.26 lm/W, and EQE = 0.3%, $V_{turn-on}$ = 5.3 V and (CIE)x,y = (0.516, 0.350) at 10 mA/cm^2. At this point of discussion, it is noteworthy to mention that a handful of organo-Sm(III) complexes has been utilized for the fabrication of OLEDs. Furthermore, it is even more important to emphasize that there is a single report on the utilization of tetrakis Sm(IIII) complex to fabricate OLEDs [26b]. Interestingly, most of the organo-Sm(III) complexes based OLEDs reported (**Table 4**, **Chart 3**) [26b, 35] displayed orange emission [26b, 35a-d] except for **Sm-8** (**Chart 3**), which exhibited red emission [35h].

Table 3: Key EL properties of the single- and double-EML devices of **Sm-1** operating at current density of 10 mA/cm^2.

Device	$V_{turn-on}$ (V)	B[a] (cd/m^2)	η_c[b] (cd/A)(EQE[c])	η_p[d] (lm/W)	$CIE_{x,y}$[e]
Single-EML Devices					
1	8.1	91	0.27 (0.2%)	0.09	0.627, 0.321
2	6.5	119	0.29 (0.2%)	0.13	0.554, 0.334
3	7.1	149	0.35 (0.3%)	0.15	0.613, 0.321
4	7.2	110	0.29 (0.2%)	0.14	0.623, 0.319
Double-EML Devices					
5	7.7	80	0.24 (0.2%)	0.08	0.616, 0.335
6	6.7	114	0.27 (0.2%)	0.19	0.562, 0.326
7	7.2	140	0.44 (0.3%)	0.19	0.605, 0.328
8	7.4	110	0.45 (0.3%)	0.24	0.622, 0.323

[a]The data for maximum brightness (B); [b]maximum current efficiency (η_c); [c] maximum external quantum efficiency (EQE); [d]maximum power efficiency (η_p); [e]$CIE_{x,y}$ at 10 mA/cm^2; $V_{turn-on}$ = applied voltage at the brightness of 1.0 cd/m^2

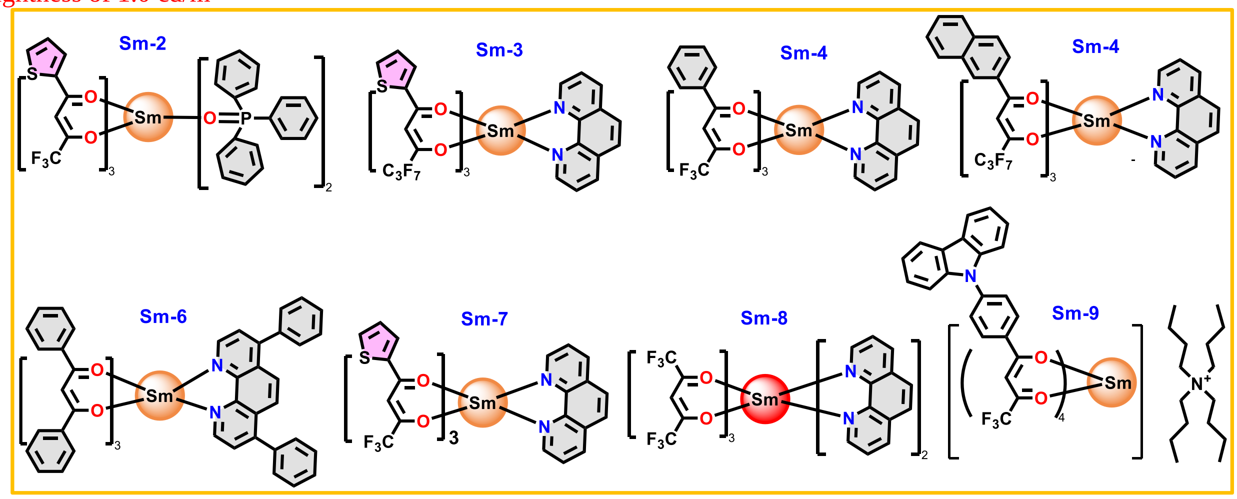

Chart 3: Chemical structures of the reported Sm(III) β-diketonate complexes utilized to fabricate OLEDs.

Table 4: EL performances of OLEDs with Sm(III) β-diketonate complexes as emitters.

Complexes	$V_{turn-on}$	B^a	$\eta_c{}^b$	η_p	Color/CIE	Ref
Sm-1	7.1	149	0.35	0.15	Pure red	**This work**
Sm-2	15	0.5 (23 V)	-	-	Orange	[35a]
Sm-3	9	21	0.114	-	Orange–red	[35g]
Sm-4	-	135 (10 V)	-	-	Reddish-orange	[35b]
Sm-5	-	43 (14 V)	0.18	-	Reddish-orange	[35c]
Sm-6	3.0	490 (15V)	-	-	Yellow	[35e]
Sm-7	-	81 (12.3 V)	0.04 (12V)	-	Orange	[35d]
Sm-5	-	118 (13.6)	0.029	0.0056	Orange	[35f]
Sm-8	-	135	0.1	-	Red	[35h]
Sm-9	7.6	831(14.9 V)	1.4(9.2 V)	0.5 (9.2 V)	Bright orange	[26b]

Conclusion

In conclusion, we have synthesized three new tetrakis lanthanide complexes and successfully applied **Sm-1** and **Eu-1** as an EML to fabricate red and orange OLEDs. The solution structure of the complexes was determined by one- and two- dimensional NMR spectroscopy, which explicitly confirm the formation of tetrakis complexes. The structure of the **Eu-1** was also established by the SC-XRD. Under the UV excitation, the **Sm-1** and **Eu-1** complexes emit their inherent bright red emission Q^L_{Sm} = 4.2 % and Q^L_{Eu} = 60.00%. However, **Tb-1** does not display its usual green emission; rather it showed almost near-white light emission $(CIE)_{x,y}$ = 0.245; 0.304 because of the presence of blue RFL. This originates from the energy mismatch (ΔE = 1,500 cm^{-1}) and thus resulted in inferior quantum yield Q^L_{Tb} = 3.8% due to in large A_{NR} rate 6.56 × 10^3 s^{-1}. Finally, **Sm-1** and **Eu-1** were utilized as emitters to fabricate single- and double-EML OLEDs through the thermal evaporation method. At the optimum doping concentration, double-EML **Eu-1** based device displayed orange emission with EL performance B = 329 cd/m^2, η_c = 0.46 cd/A, η_p = 0.26 lm/W, and EQE = 0.3%, $V_{turn-on}$ = 5.3 V and $CIE_{x,y}$ = 0.516, 0.350 at 10 mA/cm^2. While at the optimum doping concentration of 4.0 wt%, **Sm-1** based device exhibited red emission ($CIE_{x,y}$ = 0.613, 0.321) with the EL performance of B = 145 cd/m^2, η_c = 0.35 cd/A, η_p = 0.15 lm/W, EQE = 0.3% and $V_{turn-on}$ = 7.1 V.

As listed in **Table 4** and to the best of our knowledge, this is the second report on organo-Sm(III) complexes displaying red EL. The device displayed improved EL compared to the reported **Sm-8 (Chart 2)** showing red EL.

Acknowledgements

MSK acknowledges His Majesty's Trust Fund for Strategic Research (Grant No. SR/SQU/SCI/CHEM/21/01) for funding. RI thanks HM's Trust Fund for a postdoctoral fellowship. AM thanks Università di Perugia and MIUR ("Progetto AMIS – Dipartimenti di Eccellenza") for funding. LZ is grateful for the financial aid from the National Natural Science Foundation of China (21771172), Youth Innovation Promotion Association of the Chinese Academy of Sciences (2013150). WYW thanks the Hong Kong Research Grants Council (PolyU 153058/19P), Guangdong-Hong Kong-Macao Joint Laboratory of Optoelectronic and Magnetic Functional Materials (2019B121205002), Hong Kong Polytechnic University (1-ZE1C), Research Institute for Smart Energy (RISE) and the Endowed Professorship in Energy from Ms Clarea Au (847S) for the financial support. PRR is grateful to the Engineering and Physical Sciences Research Council (EPSRC) for continued funding (Grant EP/K004956/1).

Supporting Information

Experimental and basic instrumentation details; Single crystal X-ray diffraction analyses; Spectroscopic measurements and OLED device fabrication process; one and two dimensional NMR spectra of the **Eu-1** and **Tb-1**; Steady-state PL spectra, decay curves, EL data, spectra and CIE 1931 chromaticity diagrams. The cif file for the crystal structure of **Eu-1,** $[Eu(hfaa)_4][DpaH]$, has been deposited with the Cambridge Structural Database; with the CCDC Deposition Number 2141405.

References

[1] (a) Al-Busaidi IJ, Ilmi R, Zhang D, Dutra JDL, Oliveira WF, Al Rasbi NK, et al. Synthesis and photophysical properties of ternary β-diketonate europium(III) complexes incorporating bipyridine and its derivatives. Dyes Pigm. 197 (2022) pp. 109879; (b) Ilmi R, Sun W, Dutra JDL, Al-Rasbi NK, Zhou L, Qian P-C, et al. Monochromatic red electroluminescence from a homodinuclear europium(iii) complex of a β-diketone tethered by 2,2´-bipyrimidine. J.

Mater. Chem. C. 8 (2020) pp. 9816-9827; (c) Ilmi R, Kansız S, Al-Rasbi NK, Dege N, Raithby PR, Khan MS. Towards white light emission from a hybrid thin film of a self-assembled ternary samarium(iii) complex. New J. Chem. 44 (2020) pp. 5673-5683; (d) Ilmi R, Khan MS, Li Z, Zhou L, Wong W-Y, Marken F, et al. Utilization of Ternary Europium Complex for Organic Electroluminescent Devices and as a Sensitizer to Improve Electroluminescence of Red-Emitting Iridium Complex. Inorg. Chem. 58 (2019) pp. 8316-8331.

[2] Laporte O, Meggers WF. Some Rules of Spectral Structure*. J. Opt. Soc. Am. 11 (1925) pp. 459-463.

[3] (a) Ilmi R, Ganaie AB, Iftikhar K. 1H NMR of paramagnetic Lanthanide(III) complexes of trifluoroacetylacetone and 2,2´-Bipyridyl and 4f-4f absorption studies. J. Mol. Struct. 1173 (2018) pp. 990-999; (b) Ilmi R, Iftikhar K. Synthesis, visible light absorption and luminescence of bipyrimidine bridged dinuclear lanthanide complexes of 2,4-pentanedione. Inorg. Chem. Commun. 13 (2010) pp. 1552-1557.

[4] (a) Weissman SI. Intramolecular Energy Transfer The Fluorescence of Complexes of Europium. J. Chem. Phys. 10 (1942) pp. 214-217; (b) Sabbatini N, Guardigli M, Manet I. Chapter 154 Antenna effect in encapsulation complexes of lanthanide ions. In: Karl A. Gschneidner, Jr., LeRoy E, editors. Handbook on the Physics and Chemistry of Rare Earths: Elsevier; 1996. p. 69-119; (c) Moore EG, Samuel APS, Raymond KN. From Antenna to Assay: Lessons Learned in Lanthanide Luminescence. Acc. Chem. Res. 42 (2009) pp. 542-552.

[5] (a) Al-Busaidi IJ, Ilmi R, Dutra JDL, Oliveira WF, Haque A, Al Rasbi NK, et al. Utilization of a Pt(ii) di-yne chromophore incorporating a 2,2'-bipyridine-5,5'-diyl spacer as a chelate to synthesize a green and red emitting d-f-d heterotrinuclear complex. Dalton Trans. 50 (2021) pp. 1465-1477; (b) Bottrill M, Kwok L, Long NJ. Lanthanides in magnetic resonance imaging. Chem. Soc. Rev. 35 (2006) pp. 557-571.

[6] (a) Ilmi R, Zhang D, Dutra JDL, Dege N, Zhou L, Wong W-Y, et al. A tris β-diketonate europium(III) complex based OLED fabricated by thermal evaporation method displaying efficient bright red emission. Org. Electron. 96 (2021) pp. 106216; (b) Khan MS, Ilmi R, Sun W, Dutra JDL, Oliveira WF, Zhou L, et al. Bright and efficient red emitting electroluminescent devices fabricated from ternary europium complexes. J. Mater. Chem. C. 8 (2020) pp. 5600-5612; (c) Wang L, Zhao Z, Wei C, Wei H, Liu Z, Bian Z, et al. Review on the Electroluminescence Study of Lanthanide Complexes. Adv. Opt. Mater. 0 (2019) pp. 1801256; (d) Xu H, Sun Q, An Z, Wei Y, Liu X. Electroluminescence from europium(III) complexes. Coord. Chem. Rev. 293–294 (2015) pp. 228-249.

[7] (a) Yanagisawa K, Kitagawa Y, Nakanishi T, Seki T, Fushimi K, Ito H, et al. A Luminescent Dinuclear EuIII/TbIII Complex with LMCT Band as a Single-Molecular Thermosensor. Chem. Eur. J. 24 (2018) pp. 1956-1961; (b) Brites CDS, Millán A, Carlos LD. Chapter 281 - Lanthanides in Luminescent Thermometry. In: Jean-Claude B, Vitalij K P, editors. Handbook on the Physics and Chemistry of Rare Earths: Elsevier; 2016. p. 339-427.

[8] Kaczmarek AM, Liu Y-Y, Wang C, Laforce B, Vincze L, Van Der Voort P, et al. Lanthanide "Chameleon" Multistage Anti-Counterfeit Materials. Adv. Funct. Mater. 27 (2017) pp. 1700258.

[9] (a) Bünzli J-CG, Wong K-L. Lanthanide mechanoluminescence. J. Rare Earths. 36 (2018) pp. 1-41; (b) Bünzli J-CG. Rising Stars in Science and Technology: Luminescent Lanthanide Materials. Eur. J. Inorg. Chem. 2017 (2017) pp. 5058-5063.

[10] Binnemans K. Rare-earth beta-diketonates. In: K.A. Gschneidner JCB, Pecharsky VK, editors. Handbook on the Physics and Chemistry of Rare Earths: Elsevier; 2005. p. 107-272.

[11] Marques LF, Santos HP, D'Oliveira KA, Botezine NP, Freitas MCR, Freire RO, et al. New photo/electroluminescent europium(III) β-diketonate complex containing a p,p ´ -disubstituted bipyridine ligand: Synthesis, solid state characterization, theoretical and experimental spectroscopic studies. Inorg. Chim. Acta. 458 (2017) pp. 28-38.

[12] (a) Marchetti F, Pettinari C, Pizzabiocca A, Drozdov AA, Troyanov SI, Zhuravlev CO, et al. Syntheses, structures, and spectroscopy of mono- and polynuclear lanthanide complexes containing 4-acyl-pyrazolones and diphosphineoxide. Inorg. Chim. Acta. 363 (2010) pp. 4038-4047; (b) Safronova AV, Bochkarev LN, Malysheva IP, Baranov EV. Facile synthesis of rare-earth pyrazolonates by the reaction of rare-earth metals with 1-phenyl-3-methyl-4-isobutyryl-5-pyrazolone. Crystal structures of [Ln(PMIP)3]2 (Ln=Y, Gd, Tb, Er, Tm). Inorg. Chim. Acta. 392 (2012) pp. 454-458; (c) Sun O, Chen P, Li H-F, Gao T, Sun W-B, Li G-M, et al. A series of dinuclear lanthanide(iii) complexes constructed from Schiff base and β-diketonate ligands: synthesis, structure, luminescence and SMM behavior. Cryst. Eng. Comm. 18 (2016) pp. 4627-4635; (d) Dolinar BS, Gómez-Coca S, Alexandropoulos DI, Dunbar KR. An air stable radical-bridged dysprosium single molecule magnet and its neutral counterpart: redox switching of magnetic relaxation dynamics. Chem. Commun. 53 (2017) pp. 2283-2286; (e) Nikolaeva A, Nygaard R, Martynova I, Tsymbarenko D. Synthesis, structure and thermal behavior of volatile mononuclear mixed ligand complexes of rare-earth dipivaloylmethanates with diethylenetriamine. Polyhedron. 180 (2020) pp. 114373.

[13] (a) Ilmi R, Haque A, Khan MS. Synthesis and photo-physics of red emitting europium complexes: An estimation of the role of ancillary ligand by chemical partition of radiative decay rate. J. Photochem. Photobiol., A. 370 (2019) pp. 135-144; (b) de Oliveira TC, de Lima JF, Colaço MV, Jesus LT, Freire RO, Marques LF. Synthesis, characterization and

spectroscopic studies of binuclear lanthanide complexes containing the anti-inflammatory drug Ibuprofen and CH3-disubstituted bipyridine ligands: Influence of methyl group position in the photoluminescence. J. Lumin. 194 (2018) pp. 747-759.

[14] Nakamura K, Hasegawa Y, Kawai H, Yasuda N, Tsukahara Y, Wada Y. Improvement of lasing properties of europium (III) complexes by increase of emission quantum yield. Thin Solid Films. 516 (2008) pp. 2376-2381.

[15] Binnemans K. Lanthanide-Based Luminescent Hybrid Materials. Chem. Rev. 109 (2009) pp. 4283-4374.

[16] (a) Melby LR, Rose NJ, Abramson E, Caris JC. Synthesis and Fluorescence of Some Trivalent Lanthanide Complexes. J. Am. Chem. Soc. 86 (1964) pp. 5117-5125; (b) Mech A. Crystal structure and optical properties of novel (N(C2H5)4)[Nd(hfa)4(H2O)] tetrakis complex. Polyhedron. 27 (2007) pp. 393-405; (c) Bruno SM, Ferreira RAS, Almeida Paz FA, Carlos LD, Pillinger M, Ribeiro-Claro P, et al. Structural and Photoluminescence Studies of a Europium(III) Tetrakis(β-diketonate) Complex with Tetrabutylammonium, Imidazolium, Pyridinium and Silica-Supported Imidazolium Counterions. Inorg. Chem. 48 (2009) pp. 4882-4895; (d) Lunstroot K, Nockemann P, Van Hecke K, Van Meervelt L, Görller-Walrand C, Binnemans K, et al. Visible and Near-Infrared Emission by Samarium(III)-Containing Ionic Liquid Mixtures. Inorg. Chem. 48 (2009) pp. 3018-3026; (e) Papadopoulos CD, Skoulika S, Hatzidimitriou AG, Lalia-Kantouri M. Complex Salts of Lanthanide(III) Nitrates from Di-pyridylamine: Preparation, Structural, and Thermoanalytical -Investigation. Zeitschrift für anorganische und allgemeine Chemie. 638 (2012) pp. 2273-2279; (f) Martins JP, Martin-Ramos P, Coya C, Alvarez AL, Pereira LC, Diaz R, et al. Lanthanide tetrakis-β-diketonate dimers for solution-processed OLEDs. Mater. Chem. Phys. 147 (2014) pp. 1157-1164; (g) Biju S, Xu L-J, Hora Alves MA, Freire RO, Chen Z-N. Bright orange and red light-emitting diodes of new visible light excitable tetrakis-Ln-β-diketonate (Ln = Sm3+, Eu3+) complexes. New J. Chem. 41 (2017) pp. 1687-1695; (h) Wong H-Y, Lo W-S, Chan WTK, Law G-L. Mechanistic Investigation of Inducing Triboluminescence in Lanthanide(III) β-Diketonate Complexes. Inorg. Chem. 56 (2017) pp. 5135-5140; (i) Malina I, Kampars V, Belyakov S. Luminescence properties of 2-benzoyl-1,3-indandione based Eu3+ ternary and tetrakis complexes and their polymer films. Dyes Pigm. 159 (2018) pp. 655-665.

[17] (a) Parker D, Williams JAG. Getting excited about lanthanide complexation chemistry. J. Chem. Soc., Dalton Trans. (1996) pp. 3613-3628; (b) Hasegawa Y, Ohkubo T, Sogabe K, Kawamura Y, Wada Y, Nakashima N, et al. Luminescence of Novel Neodymium Sulfonylaminate Complexes in Organic Media. Angew. Chem. Int. Ed. 39 (2000) pp. 357-360.

[18] Ilmi R, Anjum S, Haque A, Khan MS. A new brilliant red emitting Eu(III) ternary complex and its transparent flexible and photostable poly(urethane) hybrid thin film for optoelectronic applications. J. Photochem. Photobiol., A. 383 (2019) pp. 111968.

[19] Valentini M, Rüegger H, Pregosin PS. Applications of Pulsed-Gradient Spin-Echo (PGSE) Diffusion Measurements in Organometallic Chemistry. Helv. Chim. Acta. 84 (2001) pp. 2833-2853.

[20] (a) Macchioni A, Ciancaleoni G, Zuccaccia C, Zuccaccia D. Determining accurate molecular sizes in solution through NMR diffusion spectroscopy. Chem. Soc. Rev. 37 (2008) pp. 479-489; (b) Sian L, Macchioni A, Zuccaccia C. Understanding the Role of Metallocenium Ion-Pair Aggregates on the Rate of Olefin Insertion into the Metal–Carbon Bond. ACS Catalysis. 10 (2020) pp. 1591-1606; (c) Oliva L, Oliva P, Galdi N, Pellecchia C, Sian L, Macchioni A, et al. Solution Structure and Reactivity with Metallocenes of AlMe2F: Mimicking Cation - Anion Interactions in Metallocenium–Methylalumoxane Inner-Sphere Ion Pairs. Angew. Chem., Int. Ed. 56 (2017) pp. 14227-14231; (d) Zaccaria F, Zuccaccia C, Cipullo R, Macchioni A. Extraction of Reliable Molecular Information from Diffusion NMR Spectroscopy: Hydrodynamic Volume or Molecular Mass? Chem. Eur. J. 25 (2019) pp. 9930-9937; (e) Cohen Y, Avram L, Frish L. Diffusion NMR Spectroscopy in Supramolecular and Combinatorial Chemistry: An Old Parameter—New Insights. Angew. Chem., Int. Ed. 44 (2005) pp. 520-554; (f) Avram L, Cohen Y. Diffusion NMR of molecular cages and capsules. Chem. Soc. Rev. 44 (2015) pp. 586-602; (g) Sian L, Guerriero A, Peruzzini M, Zuccaccia C, Gonsalvi L, Macchioni A. Diffusion NMR Studies on the Self-Aggregation of Ru-Arene CAP Complexes: Evidence for the Formation of H-Bonded Dicationic Species in Acetonitrile. Organometallics. 39 (2020) pp. 941-948; (h) Zuccaccia D, Macchioni A. An Accurate Methodology to Identify the Level of Aggregation in Solution by PGSE NMR Measurements: The Case of Half-Sandwich Diamino Ruthenium(II) Salts. Organometallics. 24 (2005) pp. 3476-3486.

[21] Emsley J. The composition, structure and hydrogen bonding of the β-diketones. In: Emsley J, Ernst RD, Hathaway BJ, Warren KD, editors. Complex Chemistry. Berlin, Heidelberg: Springer Berlin Heidelberg; 1984. p. 147-191.

[22] (a) Pinsky M, Avnir D. Continuous Symmetry Measures. 5. The Classical Polyhedra. Inorg. Chem. 37 (1998) pp. 5575-5582; (b) Casanova D, Llunell M, Alemany P, Alvarez S. The Rich Stereochemistry of Eight-Vertex Polyhedra: A Continuous Shape Measures Study. Chem. Eur. J. 11 (2005) pp. 1479-1494.

[23] Wagner G, Pardi A, Wuethrich K. Hydrogen bond length and proton NMR chemical shifts in proteins. J. Am. Chem. Soc. 105 (1983) pp. 5948-5949.

[24] (a) Rocchigiani L, Macchioni A. Disclosing the multi-faceted world of weakly interacting inorganic systems by means of NMR spectroscopy. Dalton Trans. 45 (2016) pp. 2785-2790; (b) Rocchigiani L, Ciancaleoni G, Zuccaccia C, Macchioni A. Probing the Association of Frustrated Phosphine–Borane Lewis Pairs in Solution by NMR Spectroscopy. J. Am. Chem. Soc. 136 (2014) pp. 112-115; (c) Zuccaccia D, Belpassi L, Tarantelli F, Macchioni A. Ion Pairing in Cationic Olefin−Gold(I) Complexes. J. Am. Chem. Soc. 131 (2009) pp. 3170-3171; (d) Pregosin PS, Kumar PGA, Fernández I. Pulsed Gradient Spin−Echo (PGSE) Diffusion and 1H,19F Heteronuclear Overhauser Spectroscopy (HOESY) NMR Methods in Inorganic and Organometallic Chemistry: Something Old and Something New. Chem. Rev. 105 (2005) pp. 2977-2998; (e) Zuccaccia C, Bellachioma G, Cardaci G, Macchioni A. Solution Structure Investigation of Ru(II) Complex Ion Pairs: Quantitative NOE Measurements and Determination of Average Interionic Distances. J. Am. Chem. Soc. 123 (2001) pp. 11020-11028; (f) Anil Kumar PG, Pregosin PS, Schmid TM, Consiglio G. PGSE diffusion, 1H–19F HOESY and NMR studies on several [Rh(1,5-COD)(Biphemp)]X complexes: detecting positional anion effects. Magn. Reson. Chem. 42 (2004) pp. 795-800; (g) Nama D, Kumar PGA, Pregosin PS, Geldbach TJ, Dyson PJ. 1H, 19F-HOESY and PGSE diffusion studies on ionic liquids: The effect of co-solvent on structure. Inorg. Chim. Acta. 359 (2006) pp. 1907-1911.

[25] Ilmi R, Iftikhar K. Synthesis and photoluminescence properties of pink luminescent heteroleptic Sm(III) complexes; the role of DMSO in transforming the inner coordination sphere and on photophysical properties. Sparkle/RM1 calculation. Polyhedron. 127 (2017) pp. 191-202.

[26] (a) Lunstroot K, Driesen K, Nockemann P, Van Hecke K, Van Meervelt L, Gorller-Walrand C, et al. Lanthanide-doped luminescent ionogels. Dalton Trans. (2009) pp. 298-306; (b) Biju S, Xu L-J, Hora Alves MA, Freire RO, Chen Z-N. Bright orange and red light-emitting diodes of new visible light excitable tetrakis-Ln-β-diketonate (Ln = Sm3+, Eu3+) complexes. New J. Chem. 41 (2017) pp. 1687-1695; (c) Biju S, Eom YK, Buenzli J-CG, Kim HK. A new tetrakis β-diketone ligand for NIR emitting LnIII ions: luminescent doped PMMA films and flexible resins for advanced photonic applications. J. Mater. Chem. C. 1 (2013) pp. 6935-6944.

[27] (a) Harada T, Tokuda K, Nishiyama K. Emission properties of Sm complexes substituted with asymmetric β-diketonato ligands in solution. J. Mol. Liq. 200 (2014) pp. 77-80; (b) Miyata K, Nakagawa T, Kawakami R, Kita Y, Sugimoto K, Nakashima T, et al. Remarkable Luminescence Properties of Lanthanide Complexes with Asymmetric Dodecahedron Structures. Chem. - Eur. J. 17 (2011) pp. 521-528.

[28] Ilmi R, Khan MS, Sun W, Zhou L, Wong W-Y, Raithby PR. A single component white electroluminescent device fabricated from a metallo-organic terbium complex. J. Mater. Chem. C. 7 (2019) pp. 13966-13975.

[29] Eliseeva SV, Ryazanov M, Gumy F, Troyanov SI, Lepnev LS, Bünzli J-CG, et al. Dimeric Complexes of Lanthanide(III) Hexafluoroacetylacetonates with4-CyanopyridineN-Oxide: Synthesis, Crystal Structure, Magnetic and Photoluminescent Properties. Eur. J. Inorg. Chem. 2006 (2006) pp. 4809-4820.

[30] Li Z, Yu J, Zhou L, Zhang H, Deng R. The optical properties and the natural lifetime calculation of a Sm(III) complex. Inorg. Chem. Commun. 11 (2008) pp. 1284-1287.

[31] Werts MHV, Jukes RTF, Verhoeven JW. The emission spectrum and the radiative lifetime of Eu3+ in luminescent lanthanide complexes. Phys. Chem. Chem. Phys. 4 (2002) pp. 1542-1548.

[32] (a) Biju S, Xu L-J, Sun C-Z, Chen Z-N. White OLEDs based on a novel EuIII-tetrakis-[small beta]-diketonate doped into 4,4[prime or minute]-N,N[prime or minute]-dicarbazolebiphenyl as emitting material. J. Mater. Chem. C. 3 (2015) pp. 5775-5782; (b) Biju S, Freire RO, Eom YK, Scopelliti R, Bunzli JC, Kim HK. A Eu(III) tetrakis(beta-diketonate) dimeric complex: photophysical properties, structural elucidation by Sparkle/AM1 calculations, and doping into PMMA films and nanowires. Inorg Chem. 53 (2014) pp. 8407-8417.

[33] Lee S, Kim H, Kim Y. Progress in organic semiconducting materials with high thermal stability for organic light-emitting devices. InfoMat. 3 (2021) pp. 61-81.

[34] (a) Sun P-P, Duan J-P, Shih H-T, Cheng C-H. Europium complex as a highly efficient red emitter in electroluminescent devices. Appl. Phys. Lett. 81 (2002) pp. 792-794; (b) Liang F, Zhou Q, Cheng Y, Wang L, Ma D, Jing X, et al. Oxadiazole-Functionalized Europium(III) β-Diketonate Complex for Efficient Red Electroluminescence. Chem. Mater. 15 (2003) pp. 1935-1937.

[35] (a) Reyes R, Hering EN, Cremona M, da Silva CFB, Brito HF, Achete CA. Growth and characterization of OLED with samarium complex as emitting and electron transporting layer. Thin Solid Films. 420-421 (2002) pp. 23-29; (b) Stathatos E, Lianos P, Evgeniou E, Keramidas AD. Electroluminescence by a Sm3+-diketonate-phenanthroline complex. Synth. Met. 139 (2003) pp. 433-437; (c) Yu J, Zhou L, Zhang H, Zheng Y, Li H, Deng R, et al. Efficient Electroluminescence from New Lanthanide (Eu3+, Sm3+) Complexes. Inorg. Chem. 44 (2005) pp. 1611-1618; (d) Deng R, Yu J, Zhang H, Zhou L, Peng Z, Li Z, et al. Photoluminescence and electroluminescence properties of a samarium complex Sm(TTA)3phen. Chem. Phys. Lett. 443 (2007) pp. 258-263; (e) Chu B, Li WL, Hong ZR, Zang FX, Wei HZ, Wang DY, et al. Observation of near infrared and enhanced visible emissions from electroluminescent devices with organo samarium(III) complex. J. Phys. D: Appl. Phys. 39 (2006) pp. 4549-4552; (f) Yu J, Zhang H, Zhou L, Deng R, Peng Z, Li Z, et al. Efficient organic electroluminescent devices based on an organosamarium complex. J. Lumin. 122-123 (2007) pp. 678-682; (g) Zheng Y, Fu L, Zhou Y, Yu J, Yu Y, Wang S, et al. Electroluminescence based on a β-diketonate ternary samarium complex. J. Mater. Chem.

12 (2002) pp. 919-923; (h) Kin Z, Kajii H, Hasegawa Y, Kawai T, Ohmori Y. Optical and electroluminescent properties of samarium complex-based organic light-emitting diodes. Thin Solid Films. 516 (2008) pp. 2735-2738.